ACADEMIC PRESS

Available online at www.sciencedirect.com

SCIENCE DIRECT®

Journal of Sound and Vibration 265 (2003) 583–608

JOURNAL OF SOUND AND VIBRATION

www.elsevier.com/locate/jsvi

Spatial resolution limits for the reconstruction of acoustic source strength by inverse methods

Y. Kim*, P.A. Nelson

Institute of Sound and Vibration Research, University of Southampton, Southampton SO17 1BJ, UK

Received 29 October 2001; accepted 24 July 2002

Abstract

One method for deducing the strength of an acoustic source distribution from measurement of the radiated field involves the inversion of the matrix of frequency response functions relating the field measurement points to the strengths of a number of point sources used to represent the source distribution. In practice, the frequency response function matrix to be inverted may very often be ill-conditioned. This ill-conditioning will also often result in an ill-posed problem and thus regularization algorithms are used to produce reasonable solutions. For this purpose, Tikhonov regularization has been applied, and generalized cross-validation (GCV) has been introduced as an effective method for determining the proper amount of regularization without prior knowledge of either the source distribution or the contaminating errors. In the present work, the emphasis is placed on the relationship between the spatial resolution of the reconstructed source distribution and the small singular values of the frequency response function matrix to be inverted. However, the use of Tikhonov regularization often suppresses the effect of small singular values and these are in turn often associated with high spatial frequencies of the source distribution. Thus, the process of regularization produces a useful estimate of the acoustic source strength distribution but with a limited spatial resolution. Furthermore, in the field of Fourier acoustics, the spatial resolution of the reconstructed source distribution is usually limited by the wavelength of the radiation. This paper expresses the relationship between estimation accuracy, spatial resolution, noise-level and source/sensor geometry, when a range of inverse sound radiation problems are regularised using Tikhonov regularization with GCV. The results presented form the basis of guidelines that enable the reconstruction of acoustic source strength with a resolution that is finer than the intrinsic half-wavelength limit.

*Corresponding author. Tel.: +44-2380-592279; fax: +44-2380-593190.
E-mail addresses: ytk@isvr.soton.ac.uk (Y. Kim), pan@isvr.soton.ac.uk (P.A. Nelson).

0022-460X/03/$ - see front matter
doi:10.1016/S0022-460X(02)01452-9

1. Introduction

An important inverse problem in the field of acoustics is that of reconstructing the strengths of a number of sources given a model of the transmission paths from the sources to a number of sensors at which measurements are made. In dealing with this kind of the problem, an approach based on an assumed source model has shown some promise [1–4]. This technique uses *singular value decomposition* (SVD) as a primary analysis tool. The usefulness of this decomposition stems from the fact that SVD can be interpreted in terms of "spatial frequency". In the transformation process associated with SVD, it has been demonstrated [1,2] that the transformed pressures and source distribution are related by single real numbers only (i.e., the singular values) and furthermore, that very often the large singular values are associated with the "low spatial frequencies" whilst the small singular values correspond to the "high spatial frequencies". Therefore, the resolution and the accuracy of the reconstruction produced by such inversion methods will be highly dependent on how these small singular values are treated during the inversion process.

Meanwhile, Fourier-based methods can also be used in place of SVD in dealing with the same types of inverse source problem. Here, it is usually assumed that the spatial resolution in a reconstructed source distribution is limited by the wavelength of radiation, since the resolution produced by the Fourier-based method is inversely proportional to the bandwidth of the field data. In the field of digital image processing which makes use of Fourier-based methods, however, it has been proposed [5] that, in principle, the entire wavenumber spectrum can be deduced from knowledge of the spectrum over a limited range of wavenumbers. In other words, under certain conditions, an inverse method applied to farfield data, is capable of producing greater resolution than the half-wavelength limit defined by the "Rayleigh criterion" [6,7] from classical optics. This is referred to as "super-resolution" of the reconstructed image distribution. (For a summary of the literature relating to super-resolution, see Ref. [7].) Even though practical examples of the use of these techniques are rare and although significant improvement in the resolution of the reconstructed image can be expected only with very low-noise levels and careful computation [8], it is valuable to examine the equivalent acoustical inverse problem of inverting farfield data with contaminating errors in order to obtain a detailed image of the source distribution by means of the SVD.

When the approach based on the SVD is applied to inverse source problems, regularization is usually imposed to avoid unstable solutions dominated by the errors associated with small singular values. In Refs. [2–4], some regularization methods, including the determination of the proper regularization parameters without prior information, have been shown to lead to the successful reconstruction of acoustic source distributions. Through the application of the discrete Picard condition [9,10] as an important criterion for good reconstruction, it can also be shown [4] how the regularization parameters work in reconstructing acoustic source strengths. These applications of regularization methods to ill-posed acoustical inverse problems provide considerable improvement in the resolution and in the accuracy of reconstruction.

However, even though the methods for choosing proper regularization parameters will work well, the use of Tikhonov regularization [11] often suppresses the effect of small singular values in the acoustic frequency response function matrix to be inverted. These are in turn often associated with high spatial frequencies of the source distribution. This suppression, or smoothing, effect can

produce a useful estimate of the acoustic source strength distribution but with limited spatial resolution.

Therefore, this paper will firstly investigate further the use of GCV [12,13] for providing an effective method for determining regularization parameters in acoustical inverse problems. The paper will also explore the relationships between estimated accuracy and spatial resolution, noise-level and source/sensor geometry when a range of inverse sound radiation problems are treated using Tikhonov regularization with GCV. This enables guidelines to be proposed for source/sensor geometries that produce resolution of acoustic source strengths beyond the half-wavelength limit, although it is found in practice that very low signal-to-noise ratios are required in making measurements in the farfield of acoustic source distributions.

2. Regularization for the reconstruction of acoustic source strength

2.1. Introduction

An approach to inverse source problems in acoustics has been fully described in Refs. [1,2]. Here, consider a simple free field radiation problem associated with a vibrating planar surface where no other sources or obstacles exist in the exterior region. It is assumed that the real source distribution produces acoustic pressures measured at a finite number N of receiver positions where the complex pressures detected comprise the elements of the vector $\hat{\mathbf{p}}$. Furthermore, it is assumed that the source strength distribution is considered to consist of the same number of discrete elements as sensors (where, the source strengths comprise a complex vector $\mathbf{q}$). Use of the simple least squares method based on the SVD shows that the reconstructed source strength vector $\mathbf{q}$ is given by [2,4]

$$\mathbf{q} = \mathbf{G}^{-1}\hat{\mathbf{p}} = \mathbf{V}\Sigma^{-1}\mathbf{U}^{\mathrm{H}}\hat{\mathbf{p}} = \sum_{i=1}^{N} \frac{\mathbf{u}_i^{\mathrm{H}}\hat{\mathbf{p}}}{\sigma_i}\,\mathbf{v}_i. \tag{1}$$

It should be noted that this analysis is conducted in the frequency domain, i.e., for example $\hat{\mathbf{p}}$ represents a complex vector of Fourier transforms of the measured acoustic pressures. The acoustic frequency response function matrix $\mathbf{G}$ (which is assumed here to be a square matrix) can be expressed in the form

$$\mathbf{G} = \mathbf{U}\Sigma\mathbf{V}^{\mathrm{H}} = \sum_{i=1}^{N} \mathbf{u}_i\sigma_i\mathbf{v}_i^{\mathrm{H}}. \tag{2}$$

The matrices $\mathbf{U}$ and $\mathbf{V}$ contain the left and the right singular vectors ($\mathbf{u}_i$ and $\mathbf{v}_i$) of the matrix $\mathbf{G}$ and the superscript H denotes Hermitian transpose. The matrix Σ is the diagonal matrix whose elements are the singular values σ_i.

In practice, however, since ill-conditioning of the matrix $\mathbf{G}$ will often result in an ill-posed problem, successful reconstruction of acoustic source distribution cannot always be guaranteed by using only the simple least squares method. Therefore, regularization algorithms are often used to produce reasonable solutions to discrete ill-posed problems. Application of Tikhonov

regularization shows that Eq. (1) can be written as [2,4]

$$\mathbf{q}_R = \mathbf{V}\Sigma_R^{-1}\mathbf{U}^{\mathrm{H}}\hat{\mathbf{p}} = \sum_{i=1}^{N}\left(\frac{\sigma_i^2}{\sigma_i^2+\beta}\right)\frac{\mathbf{u}_i^{\mathrm{H}}\hat{\mathbf{p}}}{\sigma_i}\,\mathbf{v}_i, \tag{3}$$

where the subscript R represents the regularized solution and β denotes the chosen Tikhonov regularization parameter. It is well known [2–4] that if β is determined properly the 'blow-up' in reconstruction caused by the inversion of very small singular values can be prevented. Meanwhile, determination of the appropriate regularization parameter requires knowledge of either the error contamination or the source distribution, but it is very difficult to obtain detailed estimation of these in practical applications. Generalized cross-validation (GCV) has thus been introduced since the technique does not require prior knowledge of the source strength distribution or of the contaminating noise. In such cases, the proper regularization parameter β_{GCV} is determined by minimizing the GCV function defined by

$$\beta_{GCV} = \min_{\beta}\,[GCV(\beta)] = \min_{\beta}\left[\frac{(1/N)\|\{\mathbf{I}-\mathbf{B}(\beta)\}\hat{\mathbf{p}}\|^2}{[(1/N)\ \mathrm{trace}\{\mathbf{I}-\mathbf{B}(\beta)\}]^2}\right], \tag{4}$$

where the influence matrix $\mathbf{B}(\beta)$ is given by $\mathbf{B}(\beta) = \mathbf{G}(\mathbf{G}^{\mathrm{H}}\mathbf{G}+\beta\mathbf{I})^{-1}\mathbf{G}^{\mathrm{H}}$ [2,3].

However, in order to apply the GCV technique to real-world applications, it is firstly necessary to demonstrate that GCV can determine the proper amount of regularization for a wide range of inverse sound radiation problems. In particular, contaminating errors in the measured field data represented by $\hat{\mathbf{p}}$ are inevitable in practical applications and hence Tikhonov regularization by the use of GCV is required to filter out the influence of the errors. In Eq. (1), for example, if the magnitude of $|\mathbf{u}_i^{\mathrm{H}}\hat{\mathbf{p}}|$ is much greater than the associated singular value σ_i as a result of contamination of errors, $\mathbf{q}$ will be dominated by the terms in the sum corresponding to the smallest singular value. Therefore, it is very important that, in order to reconstruct the source strength distribution with accuracy, the effects of the contaminating noise on the role of the magnitude of $|\mathbf{u}_i^{\mathrm{H}}\hat{\mathbf{p}}|$ in Eq. (1) must be understood and analyzed.

These effects are described by the discrete Picard condition [5] which states that the magnitude variation of $|\mathbf{u}_i^{\mathrm{H}}\hat{\mathbf{p}}|$ must decay to zero faster than the associated singular value σ_i if $\hat{\mathbf{p}}$ is assumed to be the true complex pressure without contamination. In other words, if the magnitude variation of $|\mathbf{u}_i^{\mathrm{H}}\hat{\mathbf{p}}|$ does not satisfy the discrete Picard condition, this reconstruction will suffer from the large perturbations caused by small perturbations of $\hat{\mathbf{p}}$. In practice, it is easy to show [4] by the use of the discrete Picard condition that the efficiency of the Tikhonov regularization method depends on the proper choice of the regularization parameter β that produces a fair balance between the perturbation error and the regularization error. However, even though the application of the discrete Picard condition is more useful in practice than the condition number for investigating the efficiency of regularization methods, it also demonstrates that the resolution of source strength and the accuracy of reconstruction can only be estimated roughly by comparison between the magnitude variation of the regularized value of $|\mathbf{u}_i^{\mathrm{H}}\hat{\mathbf{p}}|$ (i.e., $|\mathbf{u}_i^{\mathrm{H}}\hat{\mathbf{p}}|(\sigma_i^2/\sigma_i^2+\beta)$) in Eq. (3)) and the variation of the associated singular value σ_i. The method cannot provide directly the qualitative and quantitative insight into the performance of the regularization method based on the actual reconstruction result.

Hence, when detailed source strengths are assumed to be known, the estimation of the mean squared error (MSE) between the true source strength distribution and Tikhonov regularized solutions for all valid regularization parameters is introduced to evaluate the effectiveness of GCV. Here, the regularization parameter β_{MSE} derived from the estimation of MSE for Eq. (3) corresponds to the minimum of the MSE function, which can be written as

$$\beta_{MSE} = \min_{\beta} \ [MSE(\beta)] = \min_{\beta} \ [E[(\mathbf{q}_R - \bar{\mathbf{q}})^{\mathrm{H}}(\mathbf{q}_R - \bar{\mathbf{q}})]], \tag{5}$$

where $\bar{\mathbf{q}}$ represents the known vector of source strengths. Consequently, by comparing two regularization parameters β_{MSE} and β_{GCV} determined by two different methods, the performance of GCV can be investigated in acoustical inverse problems.

2.2. Illustrative reconstructions by means of GCV

In order to illustrate better these points, it is useful to present some results of a simple simulation of an acoustical inverse problem. Firstly, consider a linear sensor array depicted in Fig. 1. It is assumed that only one point cylindrically radiating monopole source with unit strength is located at the centre of the source line array consisting of 11 source models with equal spacing r_{ss}. The complex pressures at the distance r_{ms} are assumed to be measured with the same number of sensors as sources in the assumed model source array. The sensor array also has equal spacing r_{mm} which is also assumed here to be equal to r_{ss}. Measurement noise was added to the 'measured' acoustic pressures and 500 random trials were used. The two-dimensional Green function is given by the zero order Hankel function. This can also be used to define the frequency response relationship between the spatial Fourier transform of the acoustic pressure and the spatial Fourier transform of the associated source distribution. The Green function can be

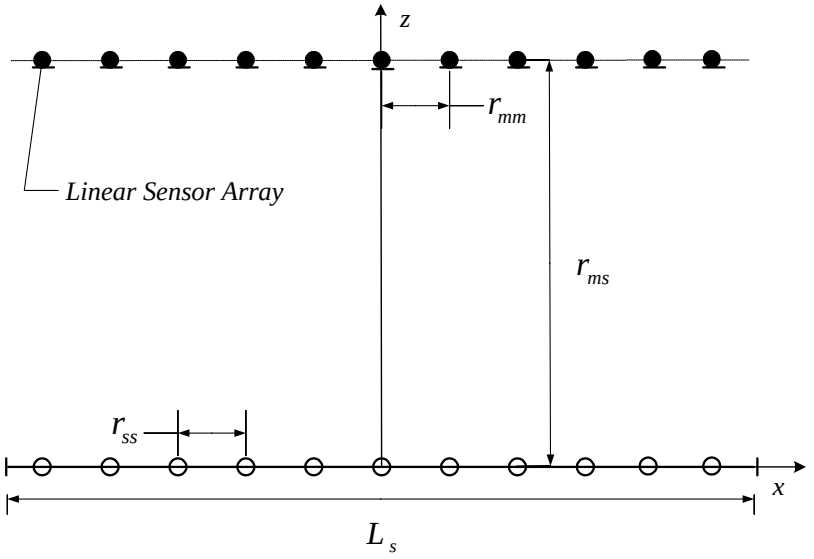

Fig. 1. The linear type of geometrical arrangement of 11 sensors and 11 sources.

written as

$$G(kr) = \frac{\omega\rho_o}{2}\mathrm{H}_o(kr), \tag{6}$$

where ρ_o is the density and the wavenumber $k = \omega/c_o$ where ω is the angular frequency and c_o is the sound speed. The Hankel function $\mathrm{H}_o(kr) = \mathrm{J}_o(kr) - j\mathrm{N}_o(kr)$, where $\mathrm{J}_o(kr)$ and $\mathrm{N}_o(kr)$ are the zeroth order Bessel and Neumann functions, respectively.

Fig. 2 illustrates the variation of the magnitude of $GCV(\beta)$ and $MSE(\beta)$ for all valid regularization parameters. Also shown is the reconstructed source strength distribution produced by Tikhonov regularization with GCV (at $\beta = \beta_{GCV}$) for illustrative acoustical conditions, in other words, a non-dimensional source spacing r_{ss}/λ where λ denotes the acoustic wavelength, a level of noise contamination $E_r = |e|/|(\hat{p} - e)|$ where e is the amplitude of the assumed noise, and a distance between the sensor array and the source array r_{ms}. When the results for β_{GCV} are compared with the value of β_{MSE}, it seems clear that GCV provides reasonable regularization parameters in the cases investigated here. This is, of course, achieved without any prior information regarding either the acoustic source strength or the contaminating measurement noise.

In order to become more sure of the use of the GCV technique in practical applications, some numerical simulations with the particular three-dimensional geometry depicted in Fig. 3 have also been performed. This geometry models a planar vibrating surface radiating to an acoustic field. Here, only one point monopole source located at the centre of the planar source array (where 9×9 source and sensor models are used) is assumed to have unit strength. The inter-sensor spacing r_{mm} is adjusted to be equal to the inter-source spacing r_{ss} and the sensor array plane is r_{ms} away from the source array plane. Measurement noise was also simulated by running 500 random trials.

As can be seen in Fig. 4, in this sensor/source arrangement, GCV still provides proper regularization parameters compared with β_{MSE}. In addition, evidence for this has already been seen and resulted in producing useful information related to the source distribution in a limited number of practical acoustic problems [2–4]. However, as can be seen in the cases investigated here (as well as that of Fig. 2), successful reconstruction cannot not always be produced even though the GCV function has determined an appropriate regularization parameter β_{GCV}. For example, in the cases of Figs. 2 (a), (b) and (d) with the linear sensor array and Figs. 4(a), (b) and (d) with the planar type sensor array, very poor reconstructions of source strengths are demonstrated. In other words, even when GCV chooses the appropriate degree in a Tikhonov regularization problem, good resolution and accuracy of reconstructed source distribution always cannot be guaranteed. Therefore, it is also valuable to investigate the resolution and the accuracy of reconstruction of the source distribution and its relationship to the acoustic conditions, for example contaminating noise level and sensor/source geometry, when dealing with a range of inverse source problems by means of GCV.

3. Spatial resolution limits for the reconstruction of acoustic source strength by inverse methods

3.1. Introduction

As described in the previous section, it is important to realize that small singular values associated with high spatial frequencies contain the fine detail, high spatial resolution information

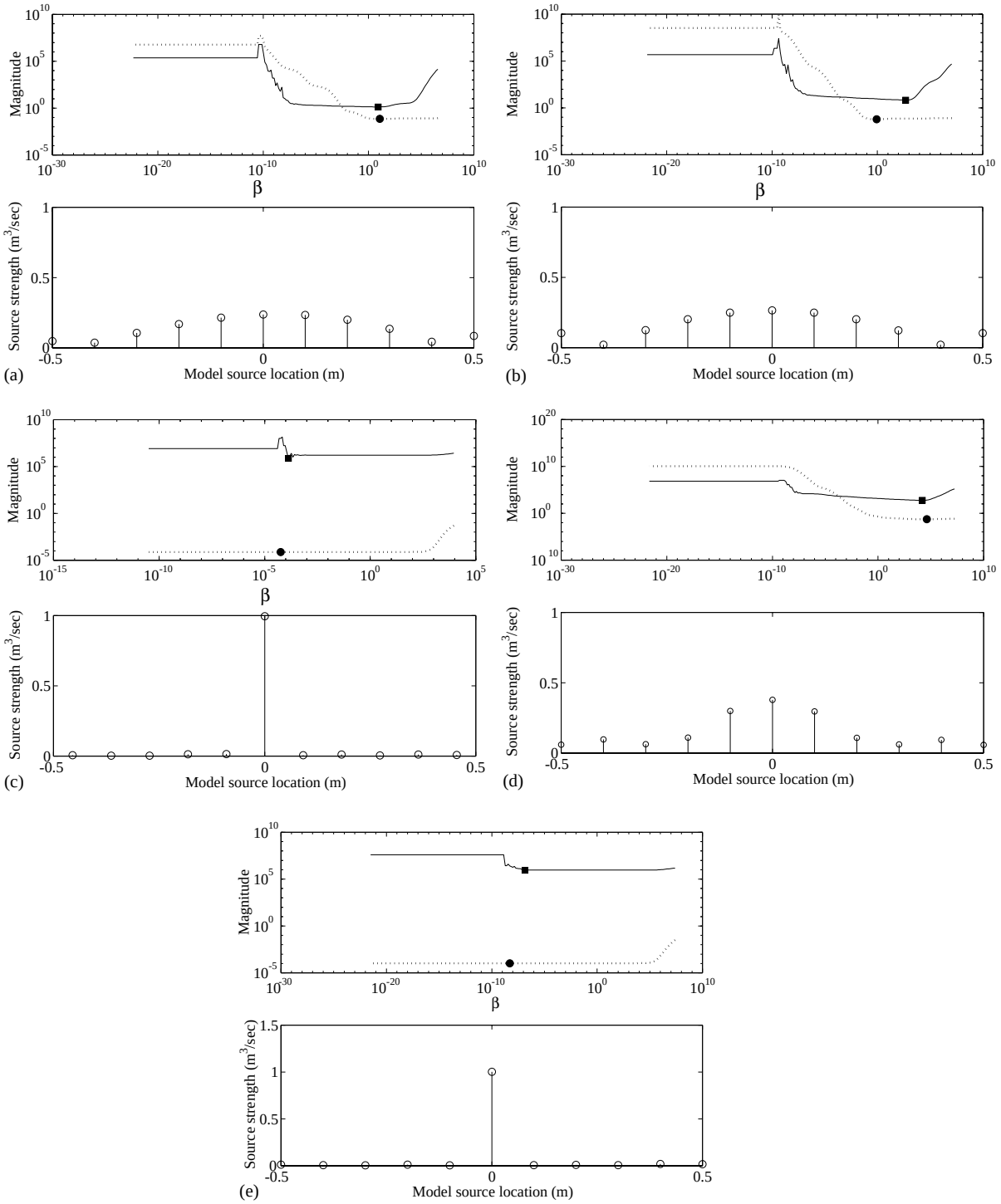

Fig. 2. Variation of the magnitude of $GCV(\beta)$ (solid line) and $MSE(\beta)$ (dotted line) for all valid regularization parameters (■: β_{GCV}, •: β_{MSE}) and the reconstructed source strength distribution produced by the Tikhonov regularization when $\beta = \beta_{GCV}$ for the linear sensor and source array: (a) $kr_{ss} = \pi/16$ ($\lambda = 3.2$ m), $E_r = 0.5$, $r_{ms} = 0.5\lambda$; (b) $kr_{ss} = \pi/2$ ($\lambda = 0.4$ m), $E_r = 0.5$, $r_{ms} = 10\lambda$; (c) $kr_{ss} = \pi$ ($\lambda = 0.2$ m), $E_r = 0.5$, $r_{ms} = 0.5\lambda$; (d) $kr_{ss} = \pi$ ($\lambda = 0.2$ m), $E_r = 0.5$, $r_{ms} = 10\lambda$; (e) $kr_{ss} = 2\pi$ ($\lambda = 0.1$ m), $E_r = 0.5$, $r_{ms} = 10\lambda$.

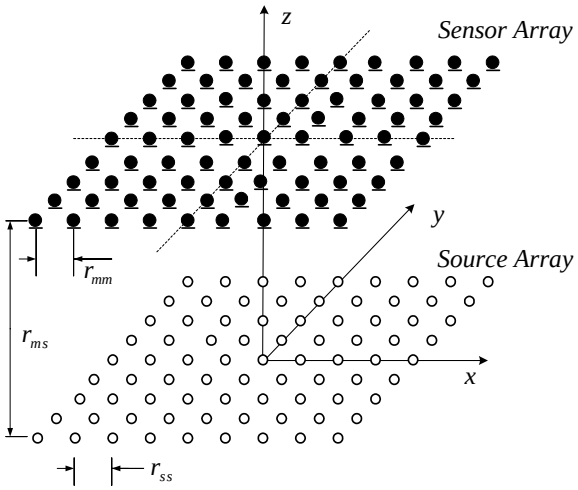

Fig. 3. The planar type sensor and source geometry (9×9 sensors and sources).

about the source. It is therefore necessary to understand spatial resolution in terms of the SVD and to establish quantitatively the extent to which the inverse method can adequately reproduce the small detail in the objects of interest.

In the field of optics, the resolution is defined by the minimum separation distance between distinguishable point objects, or the degree to which closely spaced point objects in an image can be distinguished from one another. It also is widely known in the field of classical optics [6,7] that the spatial resolution of the reconstructed image is limited by the wavelength of the radiation. In other words, the spatial resolution of the reconstructed source image is inversely proportional to the bandwidth of the field data. According to this criterion, which is known as the Rayleigh resolution criterion, two point sources can just be resolved if they are separated in an image by one half of the wavelength of the radiation. However, in the field of acoustics, super-resolution can be achieved by making measurements in the near field of a source and this has led to the development of the particular imaging technique known as Nearfield Acoustical Holography (NAH).

It has long been appreciated [14,15] in NAH that measurements undertaken in the near field of a source are capable of producing far greater resolution of the source distribution than that predicted by the classical Rayleigh criterion. However, since evanescent waves decay rapidly with the distance from the source, in order to identity these non-propagating waves associated with high spatial frequencies in the source distribution, radiation fields must be measured close to the source surface with sufficient dynamic range. Moreover, it is also well known in NAH that the spatial resolution that can be achieved is also a function of the level of contaminating noise. It has been shown, as a guideline for resolution of reconstruction by NAH, that the minimum resolvable source spacing R_{ss} is a function of the noise level and the position of the sensor array and is given by [14,15]

$$R_{ss} \approx 20\pi r_{ms}/(D \ln 10). \tag{7}$$

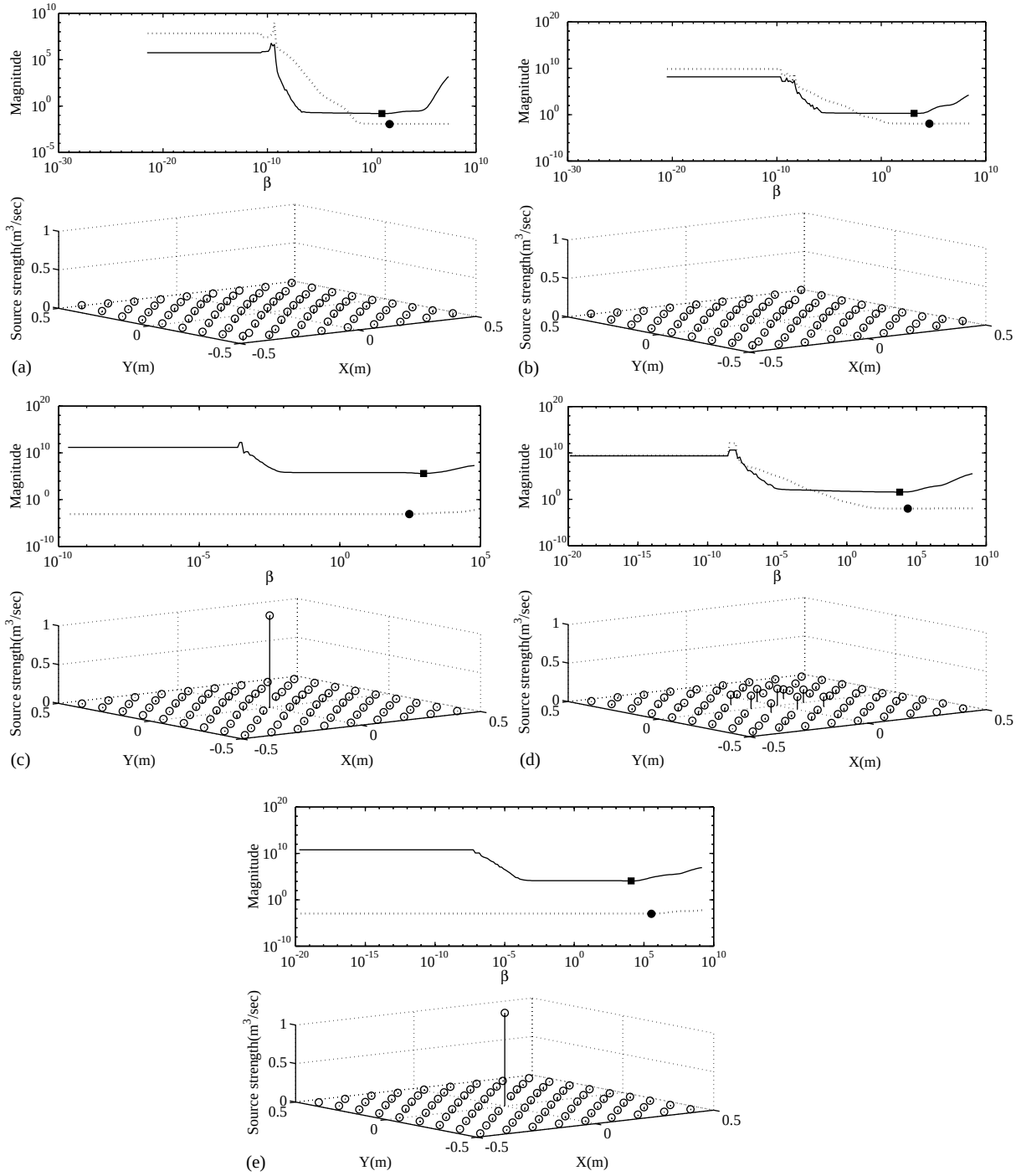

Fig. 4. Variation of the magnitude of $GCV(\beta)$ (solid line) and $MSE(\beta)$ (dotted line) for all valid regularization parameters (■:β_{GCV}, •: β_{MSE}) and the reconstructed source strength distribution produced by the Tikhonov regularization when $\beta = \beta_{GCV}$ for the planar sensor and source array: (a) $kr_{ss} = \pi/16$ ($\lambda = 3.2$ m), $E_r = 0.5$, $r_{ms} = 0.5\lambda$; (b) $kr_{ss} = \pi/2$ ($\lambda = 0.4$ m), $E_r = 0.5$, $r_{ms} = 10\lambda$; (c) $kr_{ss} = \pi$ ($\lambda = 0.2$ m), $E_r = 0.5$, $r_{ms} = 0.5\lambda$; (d) $kr_{ss} = \pi$ ($\lambda = 0.2$ m), $E_r = 0.5$, $r_{ms} = 10\lambda$; (e) $kr_{ss} = 2\pi$ ($\lambda = 0.1$ m), $E_r = 0.5$, $r_{ms} = 10\lambda$.

Here, the dynamic range D that may characterize the noise level is defined by $D = 20 \log_{10}(M/E)$, where, M is the maximum amplitude of the measured acoustic pressure and E is the amplitude of the noise. According to Eq. (7), good resolution will be obtained by having a precise measurement system with large dynamic range D and by measuring as close to the sources as possible.

This analogy for the spatial resolution may also apply to the more general formulation provided by the inverse method based on the SVD. The reason for ill-conditioning can be interpreted in terms of small singular values associated with high spatial frequencies. Furthermore, as described in Section 1, if it is possible at least in principle to produce super-resolution from farfield data [5], it should also be possible to achieve this by using inverse methods based on the SVD.

3.2. Resolution limits for the reconstruction in the near field by the inverse method

Firstly consider how the spatial resolution can be quantified. In this paper, as a measure of the spatial resolution, the Abbe distance [16,17] associated with the point spread function (PSF) of an imaging system has been adopted. In Fig. 5, the Abbe distance R_A is defined by the half-amplitude of the central peak of the image plane PSF which, in the two-dimensional case, is given by $\sin(kx)/kx$. The optical analogy presented in the above references can be used in connection with acoustic radiation problems. When the reconstructed acoustic source distribution is assumed to be equivalent to the discrete image plane PSF, the Abbe distance R_A, as the resolution criterion of reconstruction for acoustic source strengths, can be defined in discrete form as

$$R_A = 2n_A\Delta x, \quad \text{for the value of } n_A \text{ satisfying } |\bar{q}_{n_A}| \leqslant 0.5|q_0|, \tag{8}$$

where, as illustrated in Fig. 6, the magnitude of q_0 represents the peak value of the reconstructed acoustic source strengths and $\bar{q}_{n_A}$ is produced by taking an average with q_{n_A} and q_{-n_A}. In the case of three-dimensional problem, for example the geometrical arrangement of sensors and sources shown in Fig. 3, the average value $\bar{q}_{n_A}$ will be taken with four reconstructed source strengths around q_0. In general, the reconstructed source distribution is narrow and elongated when $R_A/\Delta x$ is small (the minimum $R_A/\Delta x$ is 2). As $R_A/\Delta x$ becomes larger, the "flatter" and "broader" the distribution of acoustic source strength becomes.

Fig. 1 shows the linear sensor array and source array (which has only one point monopole source with unit strength located at the centre of the line source array) which has been used to estimate spatial resolution limits in terms of the Abbe distance. Measurement noise has been added to the true complex pressures in order to simulate measured values. The sensor array has equal spacing r_{mm} which is assumed here to be equal to inter-source spacing r_{ss}. All the reconstructions of source strength have been produced by using the Tikhonov regularization method and regularization parameters have been determined by GCV.

Firstly, Fig. 7 shows the variation of the condition number with respect to the geometrical arrangement of sensors and sources (i.e., non-dimensional source spacing r_{ss}/λ and non-dimensional distance r_{ms}/r_{ss} between the sensor array and the source array). When the sensor array is placed in the field close to the source surface, the conditioning of the frequency response function matrix $\mathbf{G}$ is obviously improved.

Figs. 8(a)–(d) show that the variation of the Abbe distance R_A for a wide range of non-dimensional source spacing r_{ss}/λ and signal to noise ratio E_r at different sensor positions r_{ms} (i.e.,

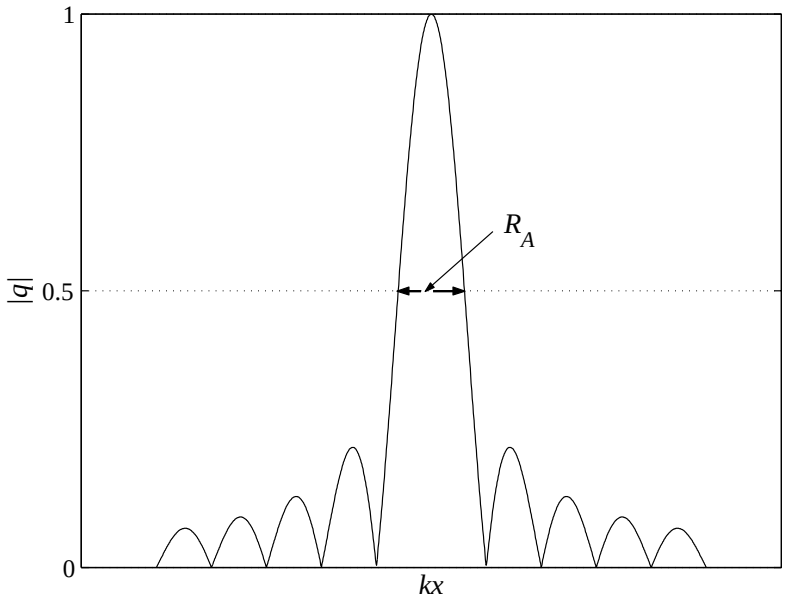

Fig. 5. The Abbe distance associated with the point spread function (PSF) of an imaging system.

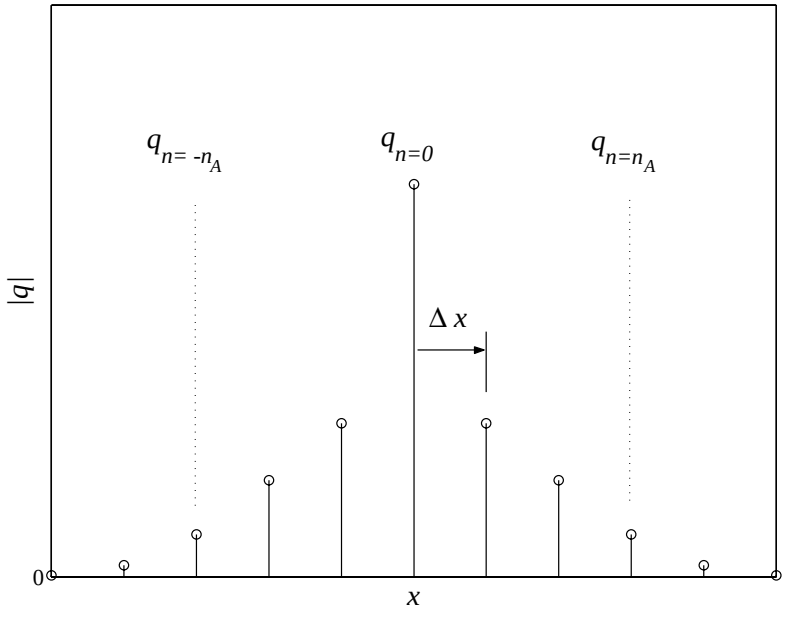

Fig. 6. The Abbe distance for a discrete acoustic source strength distribution.

r_{ms} is made equal to r_{ss}, $5r_{ss}$, $10r_{ss}$ and $10^3 r_{ss}$). In Fig. 8(a), when r_{ms} equals r_{ss} (i.e., the sensor array is placed in the field very close to the source surface), the spatial resolution of the source strength distribution is far greater than the half-wavelength resolution limit except in regions of

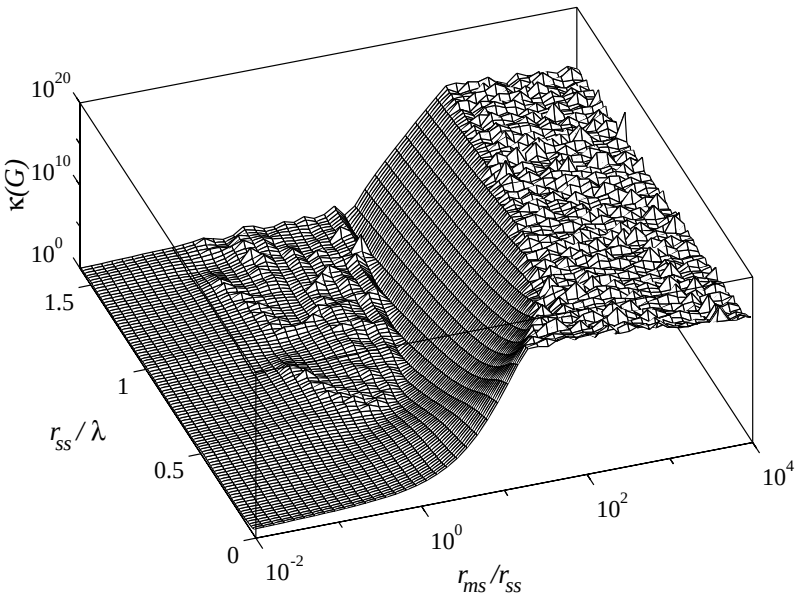

Fig. 7. The condition number variation for the linear sensor array (11 sensors and sources).

very low frequency and very high noise level. However, as the sensor array is deployed far from the source surface (i.e., as r_{ms} is increased), very poor reconstruction of the source strength distribution is found for a wide range of acoustic conditions even for very small noise levels. Hence, similar to the resolution criterion for NAH given by Eq. (7), when using the inverse method based on the SVD with the linear sensor array, the measurement must be undertaken as close as possible to the sources in order to improve the conditioning of the matrix **G**.

From the practical point of view, exploring these relationships has also been performed with the complex sensor/source geometry depicted in Fig. 3. Only one point monopole source located at the centre of the 9×9 planar source array assumed to have unit strength and the same conditions as for the linear sensor array have been used for measurement noise and the distances between the sensor array and the source array. Also, as shown in Fig. 9, the matrix **G** to be inverted will be well conditioned when measurements are undertaken close to the source array. Similarly, as shown in Figs. 10(a)–(d), when the measurements can be undertaken in the near field as close to the sources as possible, it is clear that excellent resolution of reconstruction can be produced by Tikhonov regularization with the GCV technique.

3.3. *Reconstruction from farfield data and limits to spatial resolution*

Similarly to NAH, it therefore appears from the above examples that, in order to guarantee super-resolution, it is necessary to perform measurements in the near field as close to the sources as possible. In practice, however, if the sensor array is placed close to the source surface, the acoustic pressure at the measurement position may be modified by scattering, reflection or

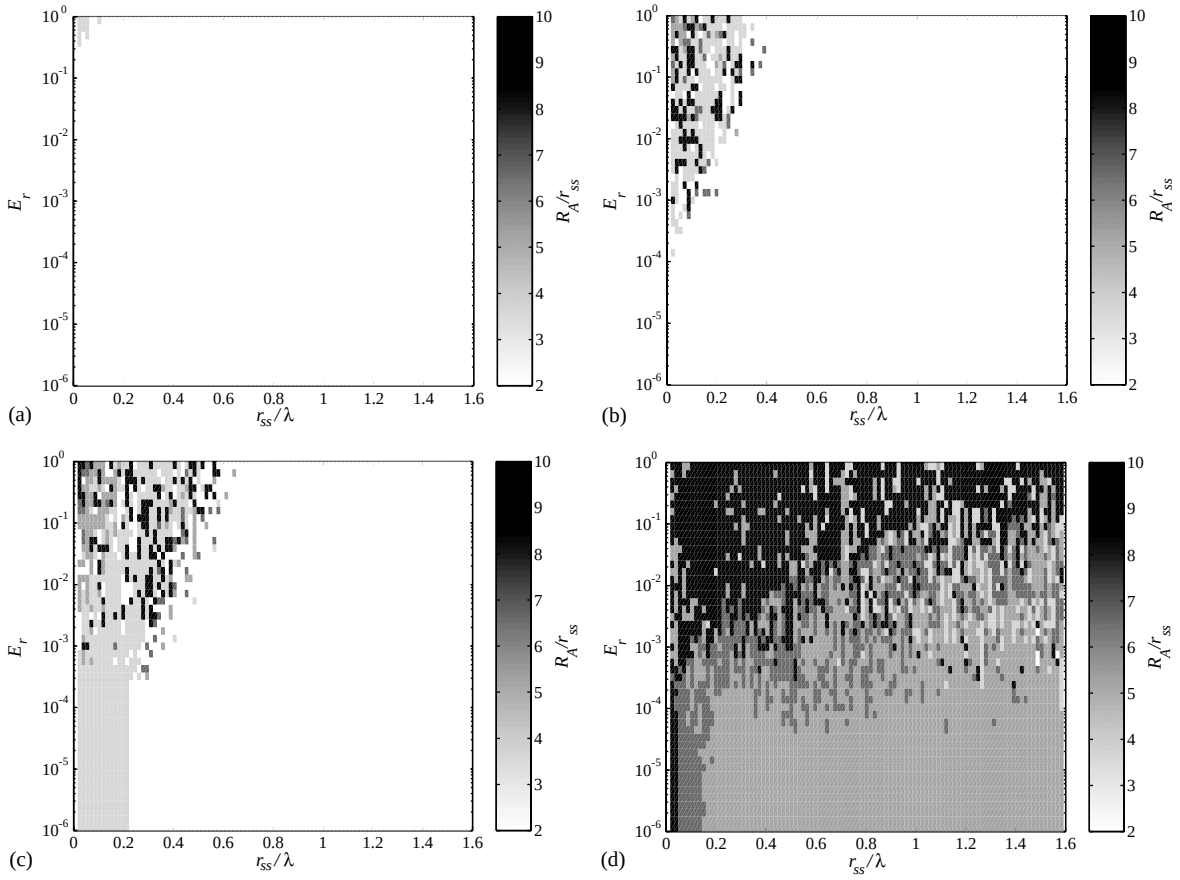

Fig. 8. Spatial resolution limits for the linear sensor array (11 sensors and sources): variation of the Abbe distance when (a) $r_{ms} = r_{ss}$, (b) $r_{ms} = 5r_{ss}$, (c) $r_{ms} = 10r_{ss}$, (d) $r_{ms} = 10^3 r_{ss}$.

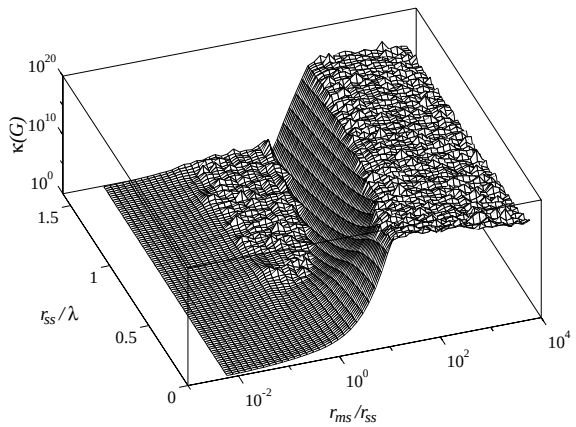

Fig. 9. The condition number variation for the planar sensor array (9×9 sensors and sources).

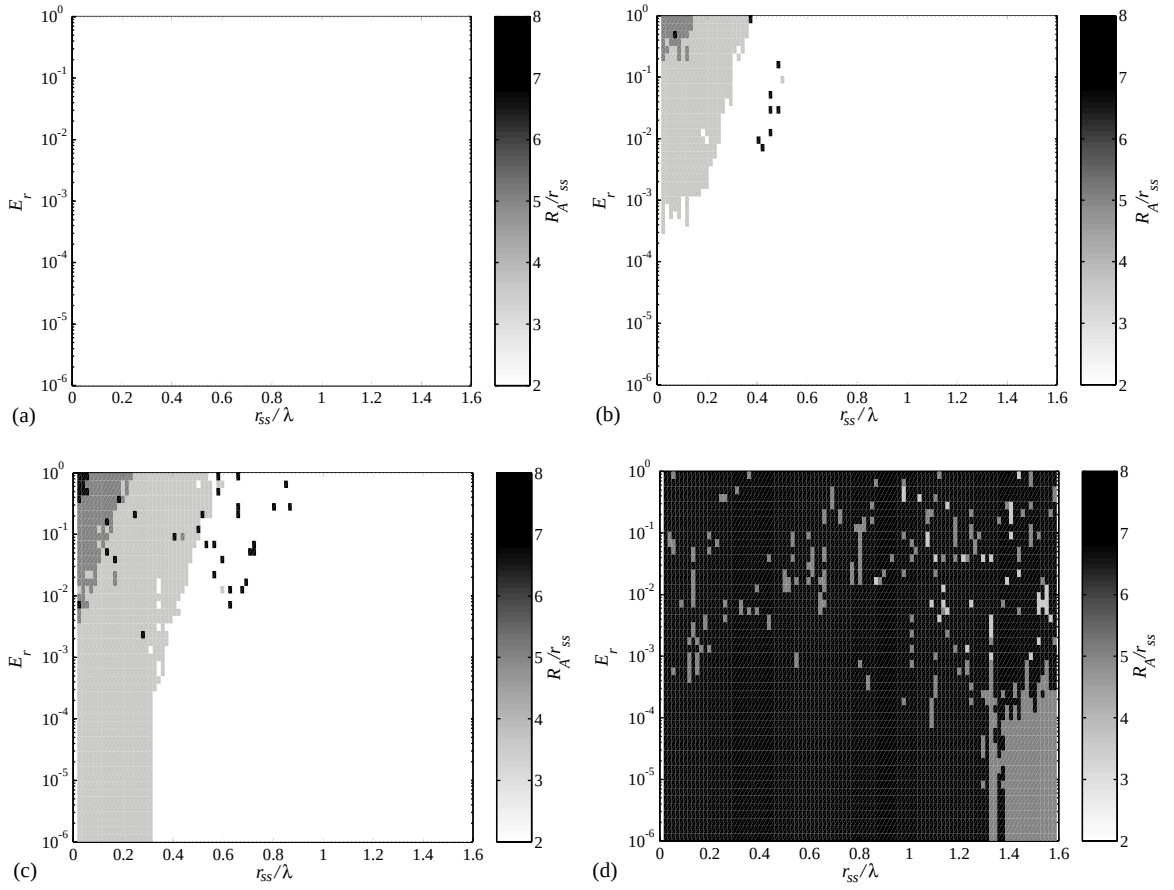

Fig. 10. Spatial resolution limits for the planar sensor array (9×9 sensors and sources): variation of the Abbe distance when (a) $r_{ms} = r_{ss}$, (b) $r_{ms} = 5r_{ss}$, (c) $r_{ms} = 10r_{ss}$, (d) $r_{ms} = 10^3 r_{ss}$.

resonance caused by the small gap between the source surface and the sensor array. Otherwise, as shown by Fig. 8(d), when the sensor array has been completely deployed to the farfield for all measured wavelengths (i.e., r_{ms} equals to $10^3 r_{ss}$), very poor reconstruction of the source strength distribution is produced over the whole range of acoustic conditions except for those with very tiny noise level. Also, in the more practical case of the three-dimensional sensor and source array (Fig. 3), very similar resolution limits at $r_{ms} = 10^3 r_{ss}$ (Fig. 10(d)) can be found to that given by the linear sensor array. However, it is already well established [2,18] that it is possible to improve the conditioning of the frequency response function matrix $\mathbf{G}$, even when acoustic source strengths are reconstructed from measurements of farfield data.

Consider the hemi-cylindrical sensor array in the farfield in Fig. 11. For the line source array, the same number of sources with the equal spacing r_{ss} as sensors has been modelled. In such cases, it follows from the Rayleigh integral and the appropriate two-dimensional Green function (given by the asymptotic form of the zero order Hankel function) that the farfield acoustic pressure can be expressed as a spatial Fourier transform of the associated source distribution. This relationship

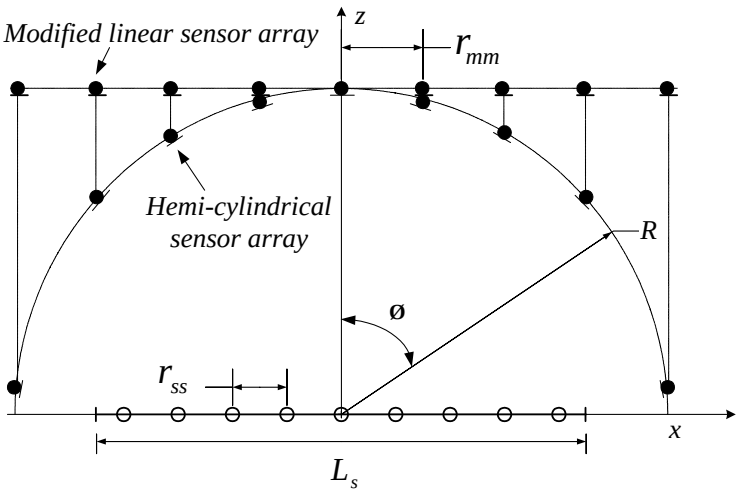

Fig. 11. The hemi-cylindrical sensor array with equal increment of $\hat{k} = k \sin\theta$ and the modified linear sensor array with equal inter-sensor spacing r_{mm}.

can be written as [19]

$$p(\mathbf{r}) = G_C(kR) \int_{-\infty}^{\infty} u_z(x) \mathrm{e}^{\mathrm{j}\hat{k}x} \mathrm{d}x, \tag{9}$$

where $G_C(kR) = \omega\rho_o \mathrm{e}^{-\mathrm{j}(kR-\pi/4)}/\sqrt{2\pi kR}$ is valid for $kR \gg 1$ (here, the wavenumber $k = \omega/c_o$, where ω is the angular frequency, c_o is the sound speed and ρ_o is the density). $u_z(x)$ is the velocity normal to the x-axis and the wavenumber variable $\hat{k} = k \sin\theta$. Sensors at the radial distance R can be spaced at equal increments of $\hat{k} = k \sin\theta$ and, as observed previously [2,4], this hemi-cylindrical sensor array results in a frequency response function matrix to be inverted that has unit condition number (i.e., the problem becomes optimally conditioned) when $r_{ss}/\lambda = 0.5$, irrespective of the number of sources assumed.

In order to consider how the sensor array can be optimally spaced, it is firstly necessary to understand the relationship between the spatial Fourier transform of the farfield data and the spatial Fourier transform of the source distribution. Here, if the source distribution in Eq. (9) is assumed to be sampled at regular intervals of r_{ss} along the x-axis, using the properties of the Dirac delta function, the sampled velocity distribution $u_{s,z}(x)$ can be expressed in the form [20]

$$u_{s,z}(x) = u_z(x) \sum_{n=-\infty}^{\infty} \delta(x - nr_{ss}). \tag{10}$$

The Fourier transform of the source strength distribution is given by

$$U_z(\mathrm{e}^{-\mathrm{j}\hat{k}r_{ss}}) = \int_{-\infty}^{\infty} u_{s,z}(x) \mathrm{e}^{-\mathrm{j}\hat{k}r_{ss}} \, \mathrm{d}x \tag{11}$$

and thus when the velocity distribution is sampled

$$U_z(\mathrm{e}^{-\mathrm{j}\hat{k}r_{ss}}) = \int_{-\infty}^{\infty} \left[u_z(x) \sum_{n=-\infty}^{\infty} \delta(x - nr_{ss}) \right] \mathrm{e}^{-\mathrm{j}\hat{k}r_{ss}}\, \mathrm{d}x, \tag{12}$$

this therefore reduces to

$$U_z(\mathrm{e}^{-\mathrm{j}\hat{k}r_{ss}}) = \sum_{n=-\infty}^{\infty} u_z(nr_{ss})\mathrm{e}^{\mathrm{j}\hat{k}nr_{ss}}, \tag{13}$$

where the discrete variable $u_z(nr_{ss})$ is defined by $u_z(nr_{ss}) = \int_{-\infty}^{\infty} u_z(x)\delta(x - nr_{ss})\, \mathrm{d}x$.

Similarly, the discrete Fourier transform of a source distribution of a finite length can be deduced (see, for example, Ref. [20] for a discussion). In Eq. (13), if only N points, for example, are assumed to have non-zero source strength and n is assumed to vary from 0 to $(N-1)$, the discrete Fourier spectrum of the sampled source strength distribution can be expressed in the form

$$U_z(\mathrm{e}^{-\mathrm{j}\hat{k}r_{ss}}) = \sum_{n=0}^{N-1} u_z(nr_{ss})\mathrm{e}^{\mathrm{j}\hat{k}nr_{ss}}. \tag{14}$$

Now note that the spatial frequency range of $\hat{k}$ between $-k$ and k can be split into N samples for evaluation of $U_z(\mathrm{e}^{-\mathrm{j}\hat{k}r_{ss}})$ at N specific values of spatial frequency with an increment of $2\pi/Nr_{ss}$. This in turn implies that $2\pi/Nr_{ss} = 2k/N$ from which it follows that $r_{ss} = \lambda/2$ since $k = 2\pi/\lambda$. Therefore, the Fourier spectrum at each of $m(2\pi/Nr_{ss})$ values of the spatial frequency, where m is the index associated with each discrete spatial frequency chosen, can be written as

$$U_z(\mathrm{e}^{-\mathrm{j}m(2\pi/Nr_{ss})r_{ss}}) = \sum_{n=0}^{N-1} u_z(nr_{ss})\mathrm{e}^{\mathrm{j}m(2\pi/Nr_{ss})nr_{ss}}. \tag{15}$$

Since $U_z(\mathrm{e}^{-\mathrm{j}\hat{k}r_{ss}})$ is determined by the number of samples in the data length chosen, the above equation can be expressed as the discrete Fourier transform

$$U_z(m) = \sum_{n=0}^{N-1} u_z(n)\mathrm{e}^{\mathrm{j}(2\pi nm/N)}, \tag{16}$$

where the inverse transform relationship is given by

$$u_z(n) = \frac{1}{N} \sum_{m=0}^{N-1} U_z(m)\mathrm{e}^{-\mathrm{j}(2\pi nm/N)}. \tag{17}$$

Thus, using the discrete Fourier spectrum of the sampled source distribution in Eq. (16), the farfield acoustic pressure in Eq. (9) can be written as

$$p(m) = \sum_{n=0}^{N-1} G_{DC}(m,n)u_z(n), \tag{18}$$

where it should be noted that the above pair of the discrete Fourier transform relationships is valid only when $r_{ss} = \lambda/2$ and then the discrete form of the frequency response function $G_{DC}(m,n)$ $(= G_c(kR)\mathrm{e}^{-\mathrm{j}(2\pi nm/N)})$ becomes proportional to the Fourier matrix. In matrix form,

the $(N \times N)$ matrix $\mathbf{G}_{DC}$ can be expressed by

$$\mathbf{G}_{DC} = G_c(kR)\mathbf{W}, \tag{19}$$

where the Fourier matrix $\mathbf{W}$ is given by

$$\mathbf{W} = \frac{1}{\sqrt{N}} \begin{bmatrix} 1 & 1 & 1 & \bullet & \bullet & 1 & 1 \\ 1 & w & w^2 & \bullet & \bullet & w^{N-2} & w^{N-1} \\ 1 & w^2 & w^4 & \bullet & \bullet & w^{2(N-2)} & w^{2(N-1)} \\ \bullet & \bullet & \bullet & \bullet & & \bullet & \bullet \\ \bullet & \bullet & \bullet & & \bullet & \bullet & \bullet \\ 1 & w^{N-2} & w^{(N-2)2} & \bullet & \bullet & w^{(N-2)(N-2)} & w^{(N-2)(N-1)} \\ 1 & w^{N-1} & w^{(N-1)2} & \bullet & \bullet & w^{(N-1)(N-2)} & w^{(N-1)(N-1)} \end{bmatrix}, \tag{20}$$

where $w = \mathrm{e}^{\mathrm{j}(2\pi/N)}$. The Fourier matrix $\mathbf{W}$ has singular values that are all unity and thus the condition number of the Fourier matrix $\mathbf{W}$ is exactly unity. Furthermore, it is well known [21] that the Fourier matrix $\mathbf{W}$ is unitary and has the property $\mathbf{W}^{-1} = \mathbf{W}^{\mathrm{H}}$.

In Fig. 12(a), when the hemi-cylindrical sensor array (here, the same number of sensors as sources has been used) is placed in the farfield (e.g., when $r_{ms} = 10^3 r_{ss}$), the conditioning of the matrix $\mathbf{G}_{DC}$ is greatly improved when compared with the condition number variation for the linear sensor array (Fig. 7). In particular, the conditioning of the matrix $\mathbf{G}_{DC}$ becomes optimal (i.e., has a condition number of unity) when $r_{ss}/\lambda = 0.5$, irrespective of the number of sources and sensors assumed. It is also obvious that the inversion problem becomes increasingly ill-conditioned as the wavelength of the radiated sound exceeds the separation of the acoustic sources (i.e., $r_{ss}/\lambda = 0.5$ for the hemi-cylindrical sensor array). Of course, as illustrated in this figure, the conditioning of the matrix $\mathbf{G}_{DC}$ is also much improved by the adoption of the modified linear sensor array depicted in Fig. 11, which is located at the distance R from the sources with the same inter-sensor spacing r_{mm} as that of the hemi-cylindrical sensor array. In contrast to the results for the hemi-cylindrical sensor array, the problem becomes very poorly conditioned as the number of the sources assumed increases and the conditioning of the matrix $\mathbf{G}_{DC}$ is worse in a wide region of r_{ss}/λ compared with that for the hemi-cylindrical sensor array. However, since the hemi-cylindrical sensor array will have the least sensitivities to contaminating errors when $r_{ss}/\lambda = 0.5$, the array may be helpful in revealing far greater high-resolution information about the sources. This may be the case in particular in uncertain circumstances which usually occur due to practical difficulties in obtaining prior knowledge of either noise contamination or the source distribution. Thus, Fig. 12(b) shows great improvement in the spatial resolution of the acoustic source distribution (where, only one point monopole source at the centre of the line source array consisting of 11 source models is assumed to have unit strength) from the farfield data with optimally spaced sensors compared with that of Fig. 8(d). This is more clearly evident from Figs. 12(c) and (e) which illustrate that much greater resolution and accuracy of reconstruction is produced with the hemi-cylindrical sensor array than shown by the results in Figs. 12(d) and (f) that are produced by the linear sensor array under the same conditions (i.e., all acoustic and geometrical conditions are the same except for the disposition of the sensor array).

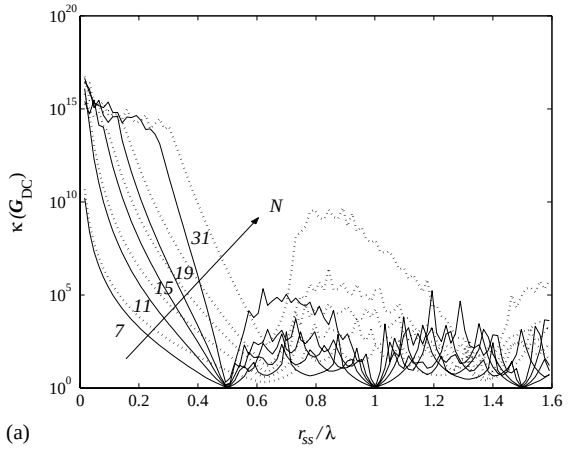
κ(G_DC)
r_ss/λ
N
31
19
15
11
7

(a)

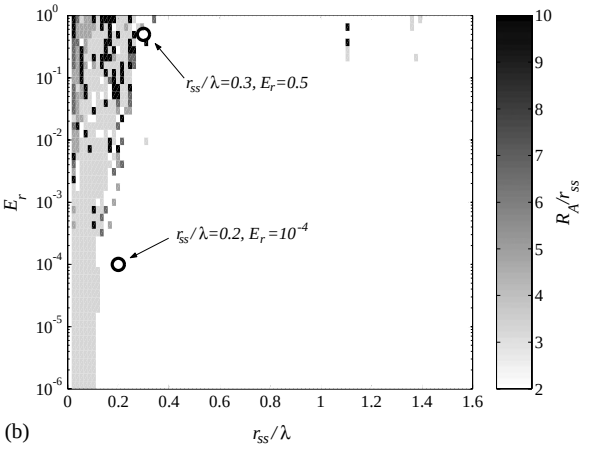
E_r
r_ss/λ
r_ss/λ=0.3, E_r=0.5
r_ss/λ=0.2, E_r=10^-4
R_A/r_ss

(b)

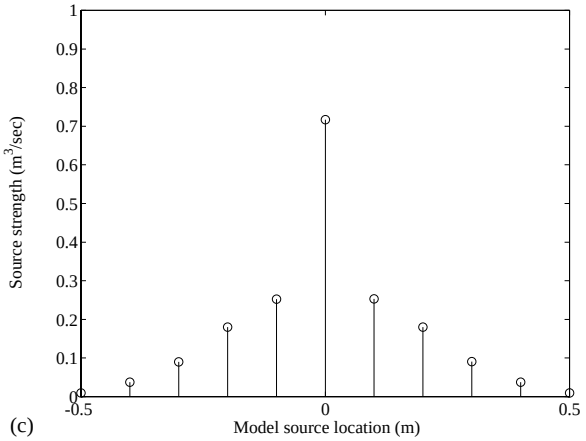
Source strength (m^3/sec)
Model source location (m)

(c)

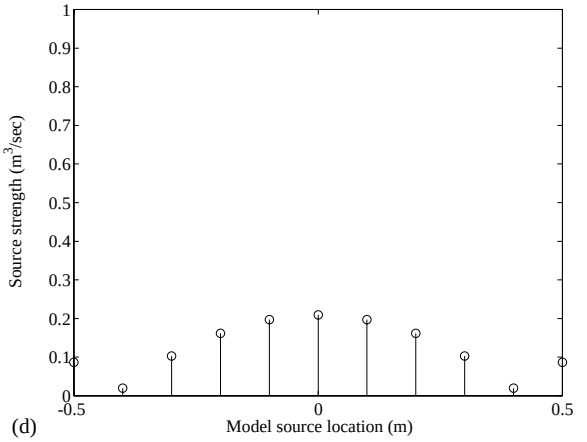
Source strength (m^3/sec)
Model source location (m)

(d)

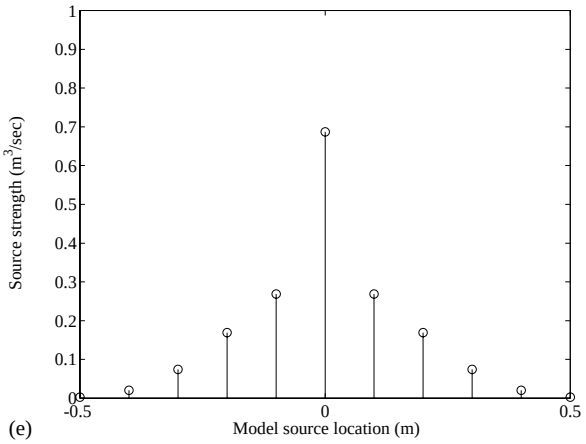
Source strength (m^3/sec)
Model source location (m)

(e)

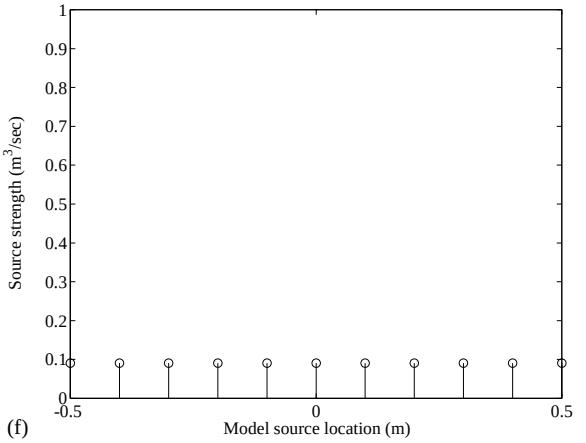
Source strength (m^3/sec)
Model source location (m)

(f)

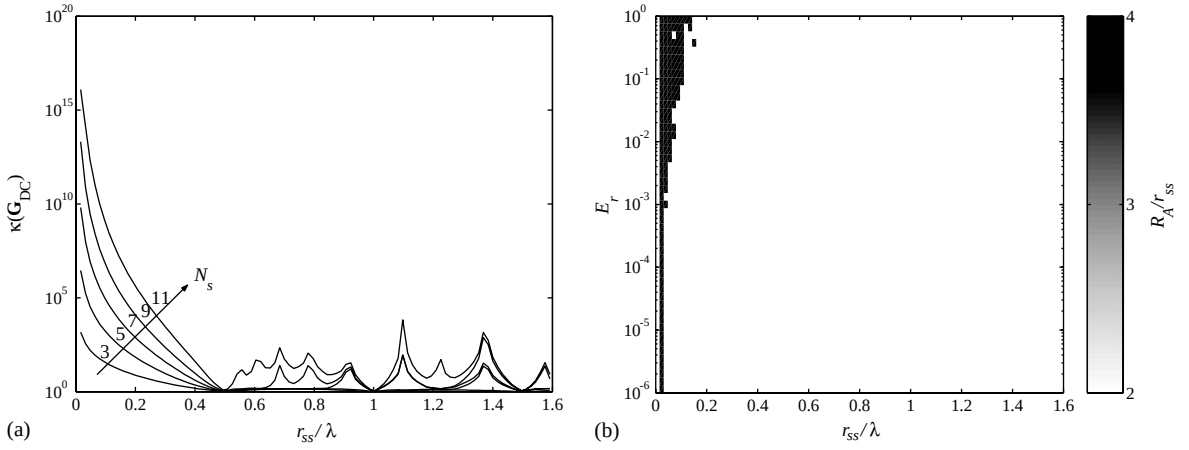

Fig. 13. The spatial resolution limits for the hemi-cylindrical sensor array with 11 sensors, when $R = 10^3 r_{ss}$: (a) variation of the condition number for the hemi-cylindrical sensor array with the number N_s of sources; (b) variation of the Abbe distance for the hemi-cylindrical sensor array with 5 sources assumed.

Furthermore, as illustrated in Fig. 13(a), the conditioning of the matrix $\mathbf{G}_{DC}$ for the hemi-cylindrical sensor array having 11 sensors is much improved, in particular in the region of the wavelength of the radiated sound which exceeds the separation of the acoustic sources (i.e., $r_{ss}/\lambda = 0.5$ for this case), when the number of sources assumed becomes smaller. Therefore, for example, when the number of sources equals to 5, it is evident from Fig. 13(b) that in this case the hemi-cylindrical sensor array produces better resolution of the acoustic source distribution compared to that for the hemi-cylindrical sensor array with 11 sources modelled.

3.4. *Reconstruction from farfield data in the three-dimensional case*

This analogy can be expanded to the three-dimensional sensor and source array. In the context of the three-dimensional example with the planar source distribution depicted in Fig. 3 (where, the $M \times N$ planar source array is assumed to have equal inter-source spacings r_{ssx}, and r_{ssy}, respectively, in the x and y directions), the three-dimensional relationship between the spatial Fourier transform of the farfield acoustic pressure and the spatial Fourier transform of the

Fig. 12. The spatial resolution limits for the hemi-cylindrical sensor array, when $R = 10^3 r_{ss}$: (a) variation of the condition number for the hemi-cylindrical sensor array (solid line) and the modified linear sensor array (dotted line); (b) variation of the Abbe distance for the hemi-cylindrical sensor array (11 sensors and sources); (c) reconstructed source strengths produced by the hemi-cylindrical sensor array (11 sensors and sources), when $r_{ss}/\lambda = 0.3, E_r = 0.5$; (d) reconstructed source strengths produced by the linear sensor array (11 sensors and sources), when $r_{ss}/\lambda = 0.3$, $E_r = 0.5$; (e) reconstructed source strengths produced by the hemi-cylindrical sensor array (11 sensors and sources), when $r_{ss}/\lambda = 0.2$, $E_r = 10^{-4}$; (f) reconstructed source strengths produced by the linear sensor array (11 sensors and sources), when $r_{ss}/\lambda = 0.2$, $E_r = 10^{-4}$.

associated planar source distribution is given by Rayleigh's first integral formula,

$$p(\mathbf{r}) = G_s(kR) \int_{-\infty}^{\infty} \int_{-\infty}^{\infty} u_z(x,y) e^{j(k_x x + k_y y)} \, dx \, dy, \tag{21}$$

where $G_s(kR) = j\omega\rho_o e^{-jkR}/2\pi R$ in the farfield (i.e., for $kR \gg 1$) and k_x, k_y are given in terms of spherical co-ordinates, i.e., $k_x = k \cos\phi \sin\theta$ and $k_y = k \sin\phi \sin\theta$. This formula shows that the farfield of any planar source is determined from the two-dimensional Fourier transform of its normal velocity distribution.

As shown in Fig. 14, the field points in the farfield are assumed to be located on the hemisphere of radius R and to have the same number as the sources in an assumed planar source array. Here, the position of the sensor on the hemisphere is determined by the upward projection from the specified position of the sensor on the source plane (i.e., $z = 0$). The relations between the sensor position on the hemisphere and the projected sensor position on the source plane can be defined by the co-ordinates $X = R \cos\phi \sin\theta$, $Y = R \sin\phi \sin\theta$ and $Z = R \cos\theta$. By using these relationships, the exponential term in Eq. (21) can be written as

$$e^{j(k_x x + k_y y)} = e^{j(k \cos\phi \sin\theta x + k \sin\phi \sin\theta y)} = e^{j(kX/R)x + (kY/R)y)}. \tag{22}$$

Similarly to the case of the hemi-cylindrical sensor array, the two-dimensional sampled velocity distribution $u_{s,z}(x,y)$ can be expressed as

$$u_{s,z}(x,y) = \sum_{n=0}^{N-1} \sum_{m=0}^{M-1} u_z(x,y)\delta(x - m r_{ssx})\delta(y - n r_{ssy}) \tag{23}$$

and the two-dimensional discrete Fourier transform of the sampled source strength can be expressed in the form

$$U_z(e^{-jk((mX/R)r_{ssx} + (nY/R)r_{ssy})}) = \sum_{m=0}^{M-1} \sum_{n=0}^{N-1} u_z(m,n) e^{jk((mX/R)r_{ssx} + (nY/R)r_{ssy})}. \tag{24}$$

Here, assuming that the acoustic pressures are sampled at equal increments of X/R and Y/R (i.e., for example, $X/R = uX_s$ and $Y/R = vY_s$ where $X_s = L_x/M$ and $Y_s = L_y/N$ in Fig. 14(b)), the exponential term in Eq. (24) can be written as

$$e^{jk((mX/R)r_{ssx} + (nY/R)r_{ssy})} = e^{jk(muX_s r_{ssx} + nvY_s r_{ssy})} = e^{jk((muL_x/RM)r_{ssx} + (nvL_y/RN)r_{ssy})} \tag{25}$$

and the superscript term in Eq. (25) will become equal to $j2\pi(mu/M + nv/N)$, provided that the inter-source spacings r_{ssx} and r_{ssy} are equal to $(R/L_x)\lambda$ and $(R/L_y)\lambda$, respectively.

Under these conditions, the final expression for the acoustic pressures in the farfield at each of $u(2\pi m/M)$ and $v(2\pi n/N)$ values of the spatial frequency, where u and v are the indices associated with each discrete spatial frequency chosen, can be written as

$$p(u,v) = \sum_{m=0}^{M-1} \sum_{n=0}^{N-1} G_{DS}(m,n,u,v) u_z(m,n), \tag{26}$$

where the discrete form of the frequency response function $G_{DS}(m,n,u,v)$ is given by

$$G_{DS}(m,n,u,v) = G_s(kR) e^{j2\pi(mu/M)} e^{j2\pi(nv/N)}. \tag{27}$$

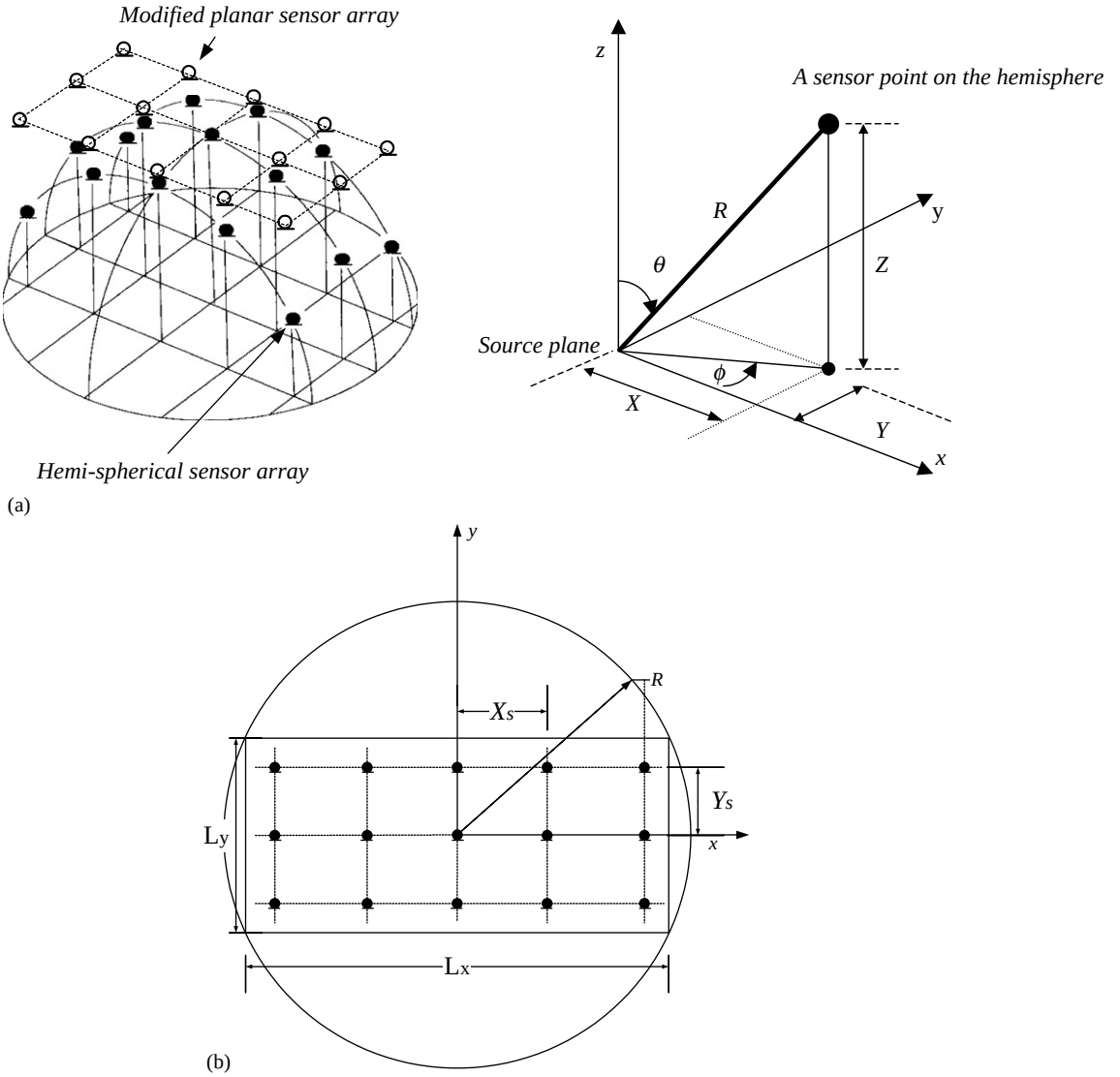

Fig. 14. The hemi-spherical sensor array with equal increments X/R and Y/R, and the modified planar sensor array (for example, 5×2 sensors and sources): (a) sensor points on the hemisphere of radius R; (b) projected positions of sensors to the source plane.

Eq. (26) exactly demonstrates a two-dimensional discrete Fourier transform relationship [7,22] between the farfield pressure and the sampled source distribution. It should be emphasized that the above relationship of the discrete Fourier transform holds only when the separation of acoustic sources r_{ssx} and r_{ssy} are equal, respectively, to $(R/L_x)\lambda$ and $(R/L_y)\lambda$.

In Eq. (26), now assume that m and u are discrete variables that range from 0 to $(M-1)$, and n and v vary from 0 to $(N-1)$. Here, since $p(u,v)$ and $u_z(m,n)$ can be row stacked to form column

vectors in order to use the same formulation as given by Eqs. (1) and (3), $p(u,v)$ and $u_z(m,n)$ can be formulated with $(MN \times 1)$ acoustic pressure and source strength vectors. Hence, $\mathbf{G}_{DS}$ can be thought of as an $(MN \times MN)$ block matrix $\mathbf{W}_B$ having M rows of M blocks and each block matrix is an $(N \times N)$ sub-matrix $\mathbf{W}$, which can be expressed as

$$\mathbf{G}_{DS} = G_s(kR)\mathbf{W}_B, \tag{28}$$

where the block matrix $\mathbf{W}_B$ is given by

$$\mathbf{W}_B = \frac{1}{\sqrt{M}}\begin{bmatrix} [\mathbf{W}] & [\mathbf{W}] & \bullet & [\mathbf{W}] & [\mathbf{W}] \\ [\mathbf{W}] & w_m[\mathbf{W}] & \bullet & w_m^{M-2}[\mathbf{W}] & w_m^{M-1}[\mathbf{W}] \\ \bullet & \bullet & \bullet & \bullet & \bullet \\ [\mathbf{W}] & w_m^{M-2}[\mathbf{W}] & \bullet & w_m^{(M-2)(M-2)}[\mathbf{W}] & w_m^{(M-2)(M-1)}[\mathbf{W}] \\ [\mathbf{W}] & w_m^{M-1}[\mathbf{W}] & \bullet & w_m^{(M-1)(M-2)}[\mathbf{W}] & w_m^{(M-1)(M-1)}[\mathbf{W}] \end{bmatrix}, \tag{29}$$

where $w_m = \mathrm{e}^{\mathrm{j}(2\pi/M)}$ and each $(N \times N)$ sub-matrix $\mathbf{W}$ is equal to the Fourier matrix from Eq. (20). The block matrix $\mathbf{W}_B$ also has the same pattern of the Fourier matrix $\mathbf{W}$ and, interestingly, the condition number is unity since all the singular values of the matrix $\mathbf{W}_B$ are units. For example, when the farfield acoustic pressures radiated from the discrete 3×2 planar source distribution are assumed to be measured by a hemi-spherical sensor array (also, assumed to be a 3×2 array) and the sources are spaced such that $r_{ssx} = (R/L_x)\lambda$ and $r_{ssy} = (R/L_y)\lambda$, the discrete Fourier transform relationship between row stacked forms of $p(u,v)$ and $u_z(m,n)$, Eq. (26) can be written in full matrix form

$$\begin{bmatrix} p(0,0) \\ p(0,1) \\ p(1,0) \\ p(1,1) \\ p(2,0) \\ p(2,1) \end{bmatrix} = \frac{G_s(kR)}{\sqrt{3}}\begin{bmatrix} [\mathbf{W}] & [\mathbf{W}] & [\mathbf{W}] \\ [\mathbf{W}] & w_m[\mathbf{W}] & w_m^2[\mathbf{W}] \\ [\mathbf{W}] & w_m^2[\mathbf{W}] & w_m^4[\mathbf{W}] \end{bmatrix}\begin{bmatrix} u_z(0,0) \\ u_z(0,1) \\ u_z(1,0) \\ u_z(1,1) \\ u_z(2,0) \\ u_z(2,1) \end{bmatrix}, \tag{30}$$

where the sub-matrix

$$\mathbf{W} = \frac{1}{\sqrt{2}}\begin{bmatrix} 1 & 1 \\ 1 & w \end{bmatrix}, \quad w = \mathrm{e}^{\mathrm{j}\pi} \text{ and } w_m = \mathrm{e}^{\mathrm{j}(2\pi/3)}.$$

In order to understand better the implication of the optimally spaced sensor in the conditioning of the matrix $\mathbf{G}_{DS}$ in Eq. (28) and the spatial resolution of reconstruction from the farfield data (for example, when $r_{ms} = 10^3 r_{ss}$), the planar sensor array in Fig. 3 has been revised based on the above guideline for optimal sensor spacing. In other words, for example the hemi-spherical sensor array, as an optimal sensor spacing, consists of the $N \times N$ sensors whose projection to the source plane is a square of dimension L (i.e., when $L = L_x = L_y$) and the $(N \times N)$ planar source array (which has equal inter-spacing $r_{ss} = r_{ssx} = r_{ssy}$) assumed as shown in Fig. 3. In such cases, since $L/R = \sqrt{2}$ (i.e., $L = 2R\cos 45^\circ$), the separation of the acoustic sources r_{ss} must be equal to $\lambda/\sqrt{2}$

in order to ensure the two-dimensional discrete Fourier transform relation between the acoustic pressure in the farfield and the $N \times N$ source distribution.

Similarly to the two-dimensional case, the problem does not become optimally conditioned as shown in Fig. 15(a) even when using a planar type of sensor array as depicted in Fig. 14. This has the same inter-sensor spacing r_{mm} as that of the hemi-spherical sensor array, but the conditioning of the matrix $\mathbf{G}_{DS}$ for the modified planar sensor array becomes much poorer as the number of sensors and sources assumed increases. However, by the adoption of the hemi-spherical sensor array, the conditioning of the matrix $\mathbf{G}_{DS}$ becomes optimal when $r_{ss} = \lambda/\sqrt{2}$ (when $r_{ms} = 10^3 r_{ss}$), irrespective of any range of $(N \times N)$ sources and sensors assumed, and is also greatly improved compared with the condition number variation of the planar sensor array of Fig. 9. Therefore, as shown in Fig. 15(b), very good spatial resolution of the reconstructed source distribution from the farfield data can be produced by the optimally spaced farfield sensor array when compared with that of Fig. 10(d), where the same planar source array as that depicted in Fig. 3 (i.e., 9×9 sensor and source array) has been used and only one point monopole source located at the centre of the source array is assumed to have unit strength. From the practical point of view, great resolution and accuracy of reconstruction produced by the hemi-spherical sensor array can be seen in Figs. 15(c) and (e) compared with Figs. 15(d) and (f) for the planar sensor array under the same conditions.

Also in the three-dimensional case, as the number of sources assumed decreases, the conditioning of the matrix $\mathbf{G}_{DS}$ for the hemi-spherical sensor array is obviously improved even when the wavelength of the radiated sound exceeds the separation of the acoustic sources as shown in Fig. 16(a). This results in greater improvement in the spatial resolution of the acoustic source distribution as illustrated in Fig. 16(b) when using 5×5 planar sources, compared with that for 9×9 planar sources in Fig. 15(b).

4. Conclusions

In this paper, Tikhonov regularization with the GCV technique has been applied to discrete inverse source problems in acoustics. It has been shown that GCV can determine proper regularization parameters in the cases investigated without prior knowledge of either the acoustic sources or the contaminating measurement noise for a wide range of conditions. However, in spite of the proper choice of the regularization parameter by the use of GCV, it has been shown that a successful reconstruction with fine resolution and reasonable accuracy cannot always be guaranteed. The limits of resolution of a number of practical source/sensor geometries have been identified by exploring the important relations between the spatial resolution, the accuracy of reconstruction and the acoustic measurement conditions. The Abbe distance has been introduced as a measure of the spatial resolution. Generally, it has been known that spatial resolution limits can be overcome by undertaking measurements in the field close to sources. However, it has also been shown that great improvement in spatial resolution of acoustic source distribution can be achieved when sensor and source geometry is optimally arranged, even when the sensor array has been completely deployed to the farfield. Furthermore, in principle, super-resolution beyond the half-wavelength limit appears possible when the strengths of a relatively small number of the sources are reconstructed with the optimally spaced sensors proposed. In practice, however, the

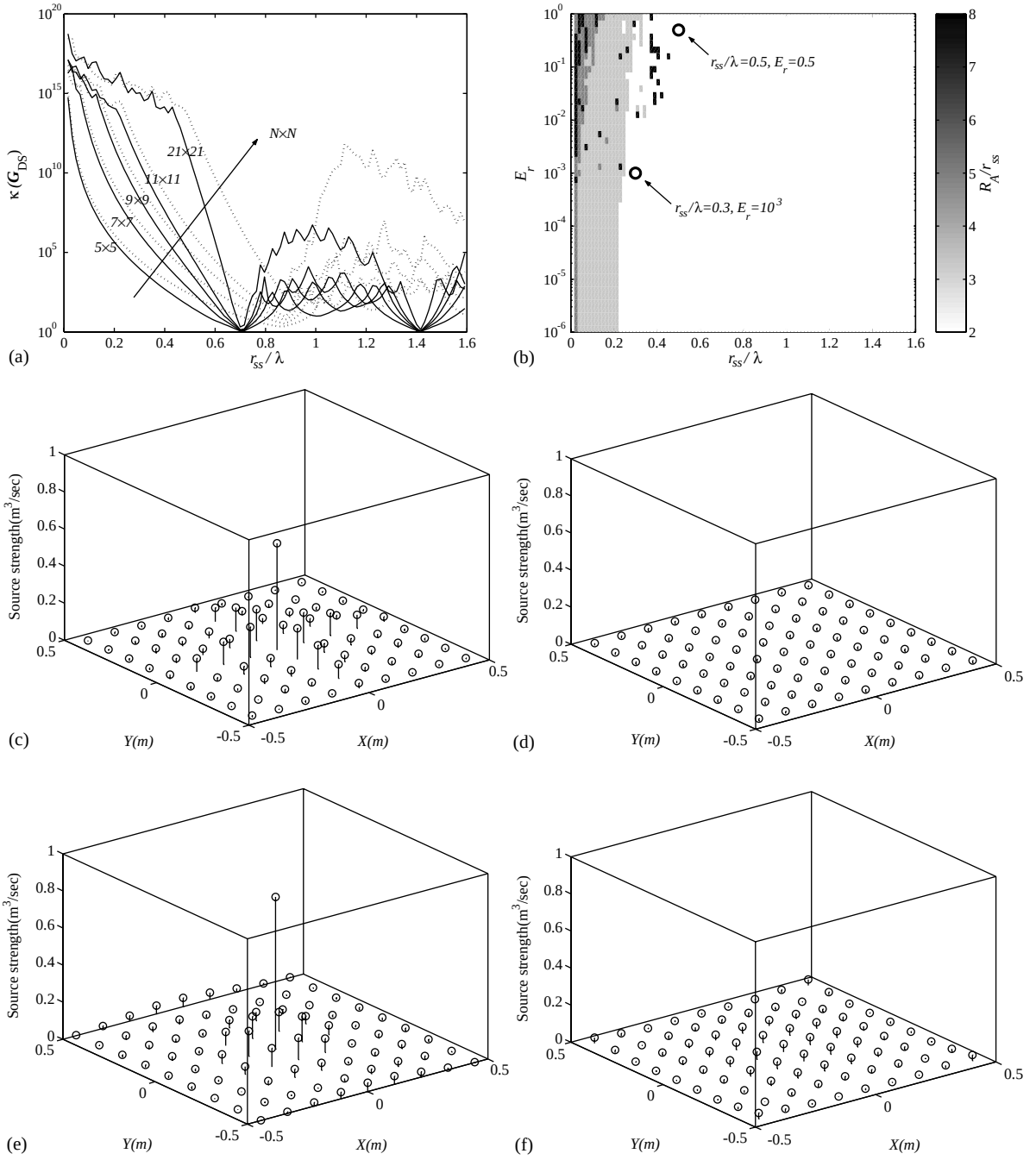

Fig. 15. The spatial resolution limits for the hemi-spherical sensor array, when $R = 10^3 r_{ss}$: (a) variation of the condition number for the hemi-spherical sensor array (solid line) and the modified planar sensor array (dotted line); (b) variation of the Abbe distance for the hemi-spherical sensor array (9×9 sources and sensors); (c) reconstructed source strengths produced by the hemi-spherical sensor array (9×9 sources and sensors), when $r_{ss}/\lambda = 0.5$, $E_r = 0.5$; (d) reconstructed source strengths produced by the planar sensor array (9×9 sources and sensors), when $r_{ss}/\lambda = 0.5$, $E_r = 0.5$; (e) reconstructed source strengths produced by the hemi-spherical sensor array (9×9 sources and sensors), when $r_{ss}/\lambda = 0.3$, $E_r = 10^{-3}$; (f) reconstructed source strengths produced by the planar sensor array (9×9 sources and sensors), when $r_{ss}/\lambda = 0.3$, $E_r = 10^{-3}$.

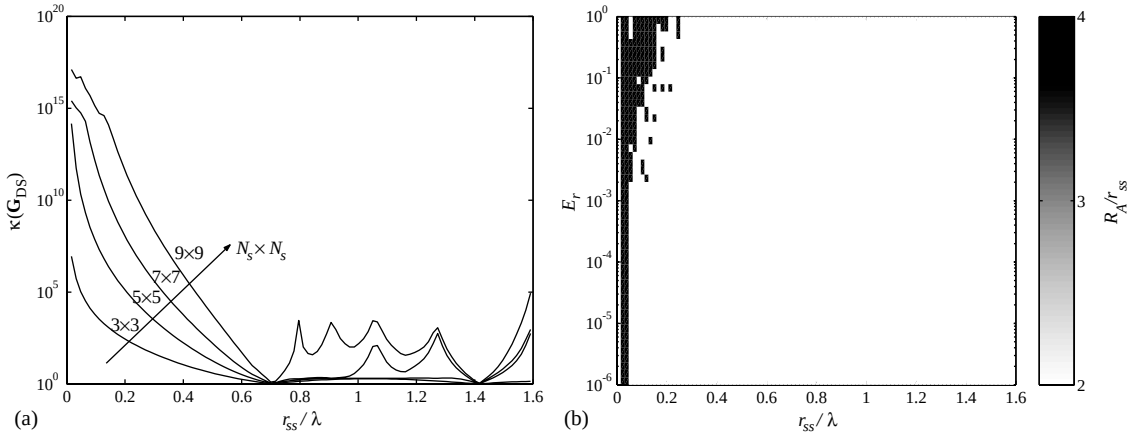

Fig. 16. The spatial resolution limits for the hemi-spherical sensor array with 9×9 sensors, when $R = 10^3 r_{ss}$: (a) variation of the condition number for the hemi-spherical sensor array with $N_s \times N_s$ planar sources; (b) variation of the Abbe distance for the hemi-spherical sensor array with 5×5 planar sources assumed.

signal-to-noise ratios associated with real measurement systems and practical numbers of the sources are unlikely to allow resolution that is significantly beyond the half-wavelength limit. These may become important guidelines for reconstructing acoustic source distributions in practical applications.

References

[1] P.A. Nelson, S.H. Yoon, Estimation of acoustic source strength by inverse methods: Part I, conditioning of the inverse problem, Journal of Sound and Vibration 233 (4) (2000) 643–668.
[2] P.A. Nelson, A review of some inverse problems in acoustics, International Journal of Acoustics and Vibration 6 (3) (2001) 118–134.
[3] S.H. Yoon, P.A. Nelson, Estimation of acoustic source strength by inverse methods: Part II, experimental investigation of methods for choosing regularization parameters, Journal of Sound and Vibration 233 (4) (2000) 665–701.
[4] Y. Kim, P.A. Nelson, Regularization methods for acoustic source reconstruction, Proceedings of InterNoise 2000 1 (2000) 128–132.
[5] J.L. Harris, Diffraction and resolving power, Journal of the Optical Society of America 54 (1964) 931–936.
[6] L. Rayleigh, On the theory of optical images, with special reference to the microscope, Philosophical Magazine 42 (1896) 167.
[7] K.R. Castleman, Digital Image Processing, Prentice-Hall, Englewood Cliffs, NJ, 1996.
[8] H.C. Andrew, H.R. Hunt, Digital Image Restoration, Prentice-Hall, Englewood Cliffs, NJ, 1977.
[9] J.M. Varah, A practical examination of some numerical methods for linear discrete ill-posed problems, SIAM Review 21 (1979) 100–111.
[10] P.C. Hansen, The discrete Picard condition for discrete ill-posed problems, BIT 30 (1990) 658–672.
[11] A.N. Tikhonov, Solution of incorrectly formulated problems and the regularization method, Soviet Mathematics DOKL 4 (1963) 1035–1038.
[12] G.H. Goulb, M. Health, G. Wahba, Generalized cross-validation as a method for choosing a good ridge parameter, Technometrices 21 (1979) 215–223.

[13] G. Wahba, Spline Models for Observation Data: CBMS-NSF Regional Conference Series in Applied Mathematics, SIAM, Philadelphia, 1990, pp. 45–65.
[14] E.G. Williams, J.D. Maynard, Holographic imaging without the wavelength resolution limit, Physics Review Letters 45 (1980) 554–557.
[15] J.D. Maynard, E.G. Williams, Y. Lee, Nearfield acoustic holography: I. Theory of generalized holography and the development of NAH, Journal of the Acoustical Society of America 78 (1985) 1395–1413.
[16] A.B. Porter, On the diffraction theory of optical images, Philosophycal Magazine 1 (1906) 154.
[17] A. Vanderlugt, Optical Signal Processing, Wiley, New York, 1992, pp. 105–110.
[18] P.A. Nelson, Y. Kim, Optimal conditioning of inverse problems in acoustic radiation, 17th International Congress on Acoustics (Book of Abstracts), Vol. 94, 2001.
[19] A.P. Dowling, J.E. Ffowcs-Williams, Sound and Sources of Sound, Ellis Horwood, Chichester, 1983.
[20] P.A. Nelson, S.J. Elliott, Active Control of Sound, Academic Press, San Diego, 1992, pp. 61–67.
[21] S. Barnett, Matrices: Methods and Applications, Oxford University Press, Oxford, 1990, pp. 342–384.
[22] B.R. Hunt, The application of constrained least squares estimation to image restoration by digital computer, IEEE Transactions on Computers C-22 (9) (1973) 805–812.